QCD Critical Point and Net-Proton Number Fluctuations at RHIC-STAR

Yu Zhang
for the STAR Collaboration
Central China Normal University
Lawrence Berkeley National Laboratory

In the search of QCD phase boundary and critical point, higher-order cumulants of conserved quantities are proposed as promising observables and have been studied extensively both experimentally and theoretically. In this paper we present cumulant ratios up-to 6^{th}-order of net-proton number distributions in Au+Au collisions at $\sqrt{s_{NN}}$= 7.7 - 200 GeV from STAR Beam Energy Scan program phase I and $\sqrt{s}$ = 200 GeV $p+p$ collisions. The results are compared with various models and Lattice QCD calculations.

1 Introduction

Quantum chromodynamics (QCD) is the theory which describes the strong interactions between quarks and gluons. It is predicted that under a very high temperature and baryon density a deconfined quark-gluon plasma (QGP) phase can be created. Studying the QCD phase structure is one of the main goals in heavy-ion collision physics. A phase diagram in terms of temperature and baryon chemical potential (μ_B) is usually used to explore the QCD phase structure. Regarding the phase transition between the QGP phase and hadronic phase, first principle Lattice QCD calculation [1] at $\mu_B = 0$ MeV suggests that the phase transition is a smooth crossover. While at large μ_B, various QCD-based models predict first order phase transition [2]. Thermodynamically there should be an end point of the first order phase boundary which is called QCD critical point. The possible QCD critical point and first order phase boundary have been investigated both experimentally and theoretically.

Higher-order cumulants of conserved quantities like net-baryon number, net-charge number and net-strangeness number are proposed as promising observables to search for the QCD critical point and the first order phase boundary. Higher-order cumulants are sensitive to the correlation length (ξ) [3,4] and are directly related to susceptibility (χ) of the system [5]. It is predicted that the fourth-order fluctuations will exhibit a non-monotonic energy dependence [6,7,8] when passing through the critical region. For 5th- and 6th-order cumulants recent calculations from Lattice QCD [9] and the functional renormalisation group approach (FRG) [10] show that they will be negative due to the crossover transition between QGP and hadronic phase. At high baryon density region, on the other hand, they are also sensitive to the 1^{th}-order phase boundary [11,12].

2 Cumulants

This section discusses cumulant definition. Let N represent conserved quantity like net-proton number from data sample. The deviation from its mean value ($\langle N\rangle$) is defined as $\delta N = N - \langle N\rangle$. Then cumulants up-to 6^{th}-order can be written as:

$$
\begin{aligned}
\mathrm{C}_1 &= \langle N\rangle,\\
\mathrm{C}_2 &= \langle(\delta N)^2\rangle,\\
\mathrm{C}_3 &= \langle(\delta N)^3\rangle,\\
\mathrm{C}_4 &= \langle(\delta N)^4\rangle - 3\langle(\delta N)^2\rangle^2,\\
\mathrm{C}_5 &= \langle(\delta N)^5\rangle - 10\langle(\delta N)^3\rangle\langle(\delta N)^2\rangle,\\
\mathrm{C}_6 &= \langle(\delta N)^6\rangle - 15\langle(\delta N)^4\rangle\langle(\delta N)^2\rangle - 10\langle(\delta N)^3\rangle^2 + 30\langle(\delta N)^2\rangle^3.
\end{aligned}
\tag{1}
$$

Various cumulant ratios like $\mathrm{C}_3/\mathrm{C}_2$, $\mathrm{C}_4/\mathrm{C}_2$, $\mathrm{C}_5/\mathrm{C}_1$ and $\mathrm{C}_6/\mathrm{C}_2$ are constructed to cancel volume effects and to readily make comparison with ratios of susceptibility (χ_n). The cumulant ratios

C_3/C_2, C_4/C_2 are also named $S\sigma$ and $\kappa\sigma^2$ respectively.

3 Analysis details

The data are collected in STAR Beam Energy Scan program phase I Au+Au collisions at $\sqrt{s_{NN}}$ = 7.7 - 200 GeV and $p+p$ collisions at $\sqrt{s}$ = 200 GeV. Protons and antiprotons are identified by the Time Projection Chamber (TPC) and Time of flight (TOF) detectors at rapidity window $-0.5 < y < 0.5$ and transverse momentum window $0.4 < p_T < 2.0$ GeV/c. At $p_T < 0.8$ GeV/c only TPC particle identification cuts are used and at $p_T > 0.8$ GeV/c additional TOF particle identification cuts are used to ensure proton purity.

The centrality is determined using charged particle multiplicity within $|\eta| < 1.0$ excluding protons and antiprotons to avoid auto-correlation effect [14]. The centrality bin width correction [14] is applied to suppress initial volume fluctuation effect. Cumulants are calculated at each multiplicity bin and then their weighted averages are taken for each centrality bin. The weight is number of events at the corresponding multiplicity bin. Detector efficiency correction [13] in cumulant calculations are done by assuming binomial detector efficiency. Statistical uncertainties of cumulants are estimated by Bootstrap and Delta methods [15].

4 Results

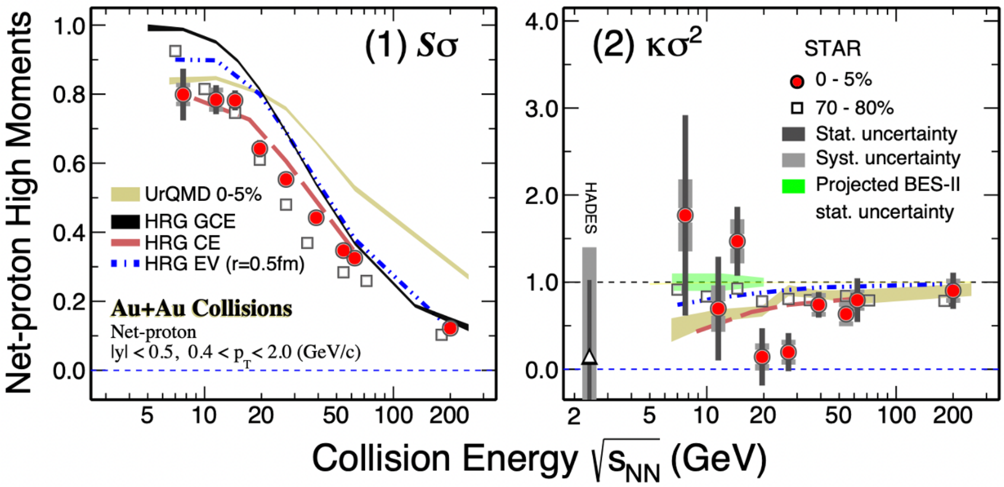

Figure 1 – Energy dependence of $S\sigma$ and $\kappa\sigma^2$ of net-proton number distributions in Au+Au collisions at $\sqrt{s_{NN}}$ = 7.7 - 200 GeV. The calculations from different variants (GCE, EV, CE) of hadron resonance gas model (HRG) and the hadronic transport UrQMD model are shown as black, red, blue bands and a gold band respectively.

Figure 1 shows energy dependence of $S\sigma$ and $\kappa\sigma^2$ of net-proton distributions from 0-5% and 70-80% centrality bins within $|y| < 0.5$ and $0.4 < p_T < 2.0$ GeV/c in Au+Au collisions at $\sqrt{s_{NN}}$ = 7.7 - 200 GeV. [18,19] The $S\sigma$ (left panel) shows a decreasing trend with the increase of collision energy both in central and peripheral collisions. The decreasing trend can be qualitatively described by HRG [16] and UrQMD [17] models. The $\kappa\sigma^2$ (right panel) shows a non-monotonic energy dependence in central collisions while peripheral collisions shows no non-monotonic energy dependence. The non-monotonic trend in central collisions is not qualitatively described by HRG and UrQMD models.

Figure 2 shows energy dependence of C_5/C_1 and C_6/C_2 of net-proton distributions from 0-40% and 70-80% centrality bins within $|y| < 0.5$ and $0.4 < p_T < 2.0$ GeV/c in Au+Au collisions at $\sqrt{s_{NN}}$ = 7.7 - 200 GeV. It is suggested from Lattice QCD and FRG calculations that 5^{th}- and 6^{th}-order cumulants show negative sign while calculations from UrQMD and HRG

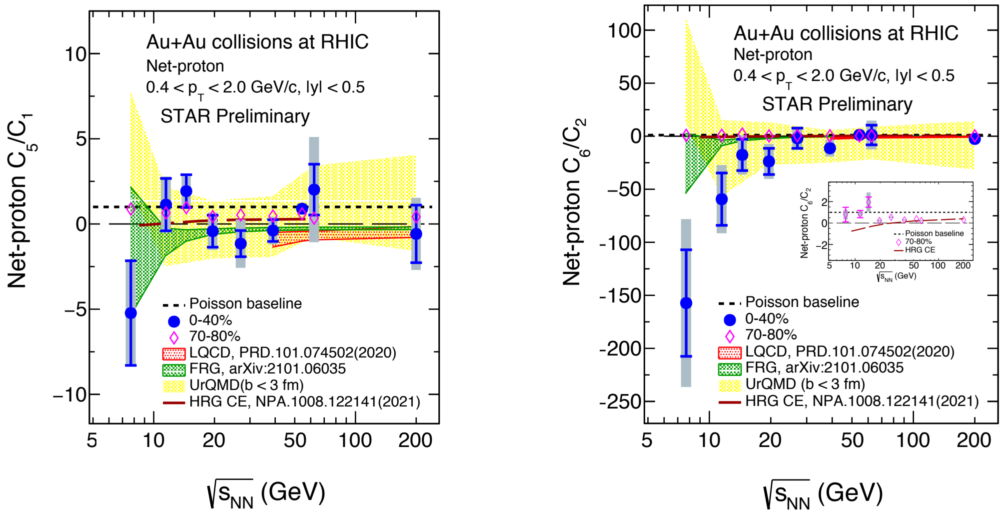

Figure 2 – Energy dependence of C_5/C_1 and C_6/C_2 of net-proton number distributions in Au+Au collisions at $\sqrt{s_{NN}}$ = 7.7 - 200 GeV. The calculations from FRG model, Lattice QCD, hadronic transport UrQMD model and Hadron Resonance Gas (HRG) model are shown as red, green and yellow bands and red lines respectively.

models are consistent with either zero or unity. In those models, no phase transition physics is implemented. The measurements of BES-I data are shown as blue dots for 0-40% and red diamonds for 70-80%. The cumulant ratio C_5/C_1 (left panel) shows negative sign at $\sqrt{s_{NN}}$ = 7.7, 19.6, 27, 39 and 200 GeV and shows positive sign at $\sqrt{s_{NN}}$ = 11.5, 14.5, 54.4 and 62.4 GeV. In peripheral collisions C_5/C_1 shows positive sign for all energies. The ratio C_6/C_2 (right panel) for 0-40% is increasingly negative with decreasing energy with less than 2σ significance while it shows positive sign in peripheral collisions (70-80%) for all energies.

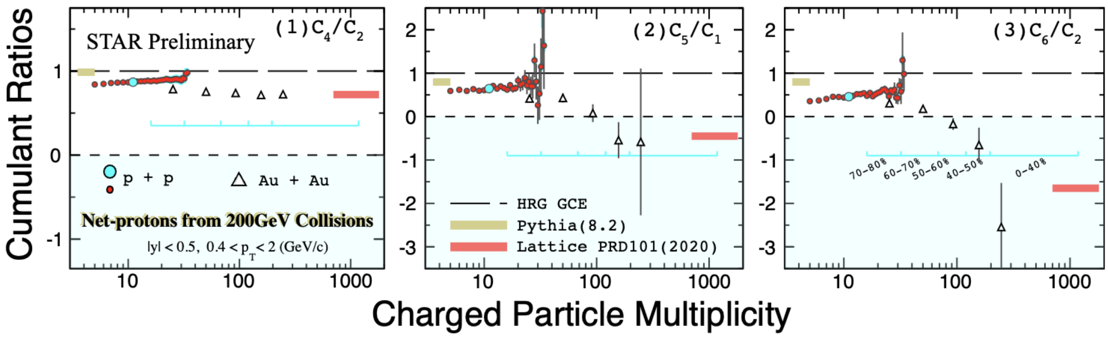

Figure 3 – Multiplicity dependence of C_4/C_2, C_5/C_1 and C_6/C_2 of net-proton number distributions in $p+p$ collisions at $\sqrt{s}$ = 200 GeV. The calculations of HRG model, Pythia (8.2) and Lattice QCD are shown as black dashed line, yellow and red bands respectively.

Figure 3 shows multiplicity dependence of net-proton results of C_5/C_1 and C_6/C_2 within $|y| < 0.5$ and $0.4 < p_T < 2.0$ GeV/c in $p+p$ collisions at $\sqrt{s}$ = 200 GeV. We see that the cumulant ratios (C_4/C_2, The cumulant ratios C_5/C_1 and C_6/C_2) from $p+p$ collisions fit into the multiplicity dependence of results from Au+Au collisions which are shown with triangles. C_5/C_1 and C_6/C_2 are negative for 0-40% in Au+Au collisions and positive at peripheral Au+Au collisions and $p+p$ collisions. Pythia [20] calculation using version 8.2 of $p+p$ collisions at $\sqrt{s}$ = 200 GeV is positive as shown with yellow bands. The Lattice QCD calculation [9] at $\sqrt{s_{NN}}$ = 200 GeV is negative as shown with red bands. Compared with calculations from various models, it is suggested that the negative sign for central Au+Au collisions at $\sqrt{s_{NN}}$ = 200 GeV is due to crossover phase transition between partonic and hadronic phases.

5 Summary

In this proceedings, we report the measurements of net-proton cumulant ratios up-to 6^{th}-order in Au+Au at $\sqrt{s_{NN}}$ = 7.7 - 200 GeV and $p + p$ collisions at $\sqrt{s_{NN}}$ = 200 GeV at STAR. With results from 200 GeV $p + p$ collisions and the energy dependence of C_4/C_2, C_5/C_1 and C_6/C_2 from the BES-I data sets, and the comparison with LQCD calculations, we conclude:

1. QCD matter is indeed created in the 200 GeV central (0-5%) Au+Au collisions at RHIC.

2. Non-monotonic energy dependence of C_4/C_2 is observed from the most central (0-5%) Au+Au collisions. [18,19]

Future results from BES-II and STAR fixed-target experiment $\sqrt{s_{NN}}$ = 3GeV data sets will allow to answer if QCD critical point exists in the covered energy region.

Acknowledgments

This work was supported by the National Key Research and Development Program of China (Grant No. 2020YFE0202002 and 2018YFE0205201), the National Natural Science Foundation of China (Grant No. 11828501, 11890711 and 11861131009) and China scholarship council (No. 201906770055).

References

1. Y. Aoki et al., *Nature* **443**, 675(2006).
2. M. Stephanov, K. Rajagopal, E. Shuryak *Phys. Rev. D* **60**, 114028(1999).
3. M. A. Stephanov, *Phys. Rev. Lett.* **102**, 032301(2009).
4. M. Asakawa, S. Ejiri, and M. Kitazawa, *Phys. Rev. Lett.* **103**, 262301(2009).
5. S. Ejiri, F. Karsch, and K. Redlich *Phys. Lett. B* **633**, 275(2006)
6. M. A. Stephanov, *Phys. Rev. Lett.* **107**, 052301(2011).
7. B.-J. Schaefer and M. Wagner, *Phys. Rev. D* **85**, 034027(2012).
8. J. Chen et al., *Phys. Rev. D* **95**, 014038(2017) and references therein.
9. A. Bazavov et al., *Phys. Rev. D* **101**, 074502(2020).
10. W. Fu et al., arXiv:2101.06035 [hep-ph].
11. A. Bzdak et al., *Phys. Rev. C* **98**, 054901(2018).
12. A. Bzdak and V. Koch, *Phys. Rev. C* **100**, 051902R(2019).
13. X. Luo, *Phys. Rev. C* **91**, 034907(2015).
14. X. Luo et al., *J. Phys. G: Nucl. Part. Phys.* **40**, 105104(2013).
15. X. Luo, *J. Phys. G: Nucl. Part. Phys.* **39**, 025008(2012).
16. P. Garg et al, *Phys. Lett. B* **726**, 691(2013).
17. M. Bleicher et al., J. Phys. G **25**, 1859(1999).
18. J. Adam et al. (STAR Collaboration), *Phys. Rev. Lett.* **126**, 092301(2021).
19. M. S. Abdallah et al. (STAR Collaboration), arXiv:2101.12413 [nucl-ex].
20. T. Sjöstrand, S. Mrenna and P. Skands, *JHEP05* (2006) **026**, *Comput. Phys. Comm.* **178** (2008) 852.